


# Tunable valley filter efficiency by spin-orbit coupling in silicene nanoconstrictions

Yi-Jian Shi(施一剑), Yuan-Chun Wang(王园春), Peng-Jun Wang(汪鹏君)

**Citation:**Chin. Phys. B, 2021, 30 (**5**): 057201. DOI: 10.1088/1674-1056/abcf35
Journal homepage: http://cpb.iphy.ac.cn; http://iopscience.iop.org/cpb

**What follows is a list of articles you may be interested in**

---

## Valley-polarized pumping current in zigzag graphene nanoribbons with different spatial symmetries

Zhizhou Yu(俞之舟), Fuming Xu(许富明)
Chin. Phys. B, 2018, 27 (**12**): 127203. DOI: 10.1088/1674-1056/27/12/127203

## Spin switching in antiferromagnets using Néel-order spin-orbit torques

P Wadley, K W Edmonds
Chin. Phys. B, 2018, 27 (**10**): 107201. DOI: 10.1088/1674-1056/27/10/107201

## Electrical controllable spin valves in a zigzag silicene nanoribbon ferromagnetic junction

Lin Zhang(张林)
Chin. Phys. B, 2018, 27 (**6**): 067203. DOI: 10.1088/1674-1056/27/6/067203

## Influence of spin-orbit coupling on spin-polarized electronic transport in magnetic semiconductor nanowires with nanosized sharp domain walls

Lian Liu(刘恋), Wen-Xiang Chen(陈文祥), Rui-Qiang Wang(王瑞强), Liang-Bin Hu(胡梁宾)
Chin. Phys. B, 2018, 27 (**4**): 047201. DOI: 10.1088/1674-1056/27/4/047201

## Spin transport in a chain of polygonal quantum rings with Dresselhaus spin-orbit coupling

Han-Zhao Tang(唐翰昭), Xiao-Teng Yao(要晓腾), Jian-Jun Liu(刘建军)
Chin. Phys. B, 2017, 26 (**11**): 117203. DOI: 10.1088/1674-1056/26/11/117203

---

# Tunable valley filter efficiency by spin–orbit coupling in silicene nanoconstrictions*

Yi-Jian Shi(施一剑), Yuan-Chun Wang(王园春), and Peng-Jun Wang(汪鹏君)†

*College of Electrical and Electronic Engineering, Wenzhou University, Wenzhou* 325035, *China*

(Received 7 July 2020; revised manuscript received 12 November 2020; accepted manuscript online 1 December 2020)

Valley filter is a promising device for producing valley polarized current in graphene-like two-dimensional honeycomb lattice materials. The relatively large spin–orbit coupling in silicene contributes to remarkable quantum spin Hall effect, which leads to distinctive valley-dependent transport properties compared with intrinsic graphene. In this paper, quantized conductance and valley polarization in silicene nanoconstrictions are theoretically investigated in quantum spin-Hall insulator phase. Nearly perfect valley filter effect is found by aligning the gate voltage in the central constriction region. However, the valley polarization plateaus are shifted with the increase of spin–orbit coupling strength, accompanied by smooth variation of polarization reversal. Our findings provide new strategies to control the valley polarization in valleytronic devices.

**Keywords:** valley polarization, spin–orbit coupling, quantization, silicene

**PACS:** 72.80.Vp, 73.22.Pr, 71.70.Ej, 73.23.–b **DOI:** 10.1088/1674-1056/abcf35

## 1. Introduction

Valleytronics has received considerable interests since the discovery of hexagonal two-dimensional materials.[1] Two inequivalent valleys located at the corners of Brillouin zone in honeycomb lattice provide a new degree of freedom for electrons, which can be used for information storage and processing. Among various valleytronic devices, valley filter and valley valve[2–5] are the most fascinating application for future electronics. Valley filters are realized in quantum point contact,[6,7] and other structures with nanobubble,[8,9] domain wall,[10,11] Corbino nanodisk[12,13] or Weyl semimetals.[14,15] In addition, mechanical,[16–18] optical,[19–21] magnetic[22–24] and electrical[25–27] methods have been applied to process valley information.

Nevertheless, it has not been extensively discussed how spin–orbit coupling (SOC) controls the valley polarization. The SOC is rather weak in graphene, while relatively strong in silicene and counterpart of other group IVA elements such as germanium and tin, due to a low-buckled structure. The SOC can be artificially engineered by adatoms or substrates, as well as changing the amplitude and stretch direction of strain.[28–31] The energy gap induced by SOC at Dirac points leads to quantum spin Hall (QSH) effect.[32–34] In this topological phase, the electronic edge state with time-reversal invariance conducts charge and spin at the sample boundaries without dissipation, which is robust against the interference of impurities and disorders.[35–37] As external staggered electric field is applied to a silicene system with a critical strength, a topological phase transition from QSH phase to trivial insulator phase occurs and the bandgap opens. To utilize this topological phase transition, topological field effect transistors have been proposed to rapidly switch between on- and off-states by tuning staggered electric field.[34,38] Furthermore, with external exchange field applied, high efficiency spin valley filters have been reported in strained silicene systems.[39,40] However, valley-dependent transport properties solely affected by larger SOC without breaking the inversion symmetry of hexagonal lattice system is still unclear and worthy of study.

In this work, we theoretically investigate the valley filter efficiency controlled by SOC in silicene nanoconstrictions. The edge orientation of the silicene lattice is zigzag type throughout the constriction. We focus on the effect of SOC that plays a vital role in manipulating the valley-dependent transport in a valley filter device. External staggered electric field and exchange field are not applied in our system, which keeps the valley filter working in QSH phase. The paper is organized as follows. In Section 2, the model and methods are introduced. Results and analysis are presented in Section 3. Conclusions are given in Section 4.

## 2. Model and methods

Valley filter device was originally proposed in graphene nanoconstriction made up of wide-narrow-wide quantum point contact.[2,3] The analogous nanoconstriction structure consisting of zigzag silicene nanoribbons is illustrated in Fig. 1. The whole open system is composed of three parts: left lead, cen-

*Project supported by the Natural Science Foundation of Zhejiang Province, China (Grant No. LQ17A040001), the National Natural Science Foundation of China (Grant Nos. 61874078, 11647046, and 61904125), the National Key Research and Development Program of China (Grant No. 2018YFB2202100), and the Science and Technology Planning Project of Wenzhou City (Grant No. G20180012).

†Corresponding author. E-mail: wangpengjun@wzu.edu.cn

© 2021 Chinese Physical Society and IOP Publishing Ltd 

tral device, and right lead. The symmetrical structure has gradual tapers with zigzag edges at the interface between leads and central device. The widths of the lead and central device are denoted by $W_Z$ and $W_C$, respectively. Meanwhile, $L$ is the length of the channel in the central device and $a = 3.86$ Å is the lattice spacing of silicene.

The Hamiltonian of the system can be described by the next-nearest-neighbor tight-binding model as follows:[29,32,34]

$$\mathcal{H} = -t\sum_{\langle i,j\rangle\alpha} c^{\dagger}_{i\alpha}c_{j\alpha} + \mathrm{i}\frac{\lambda_{SO}}{3\sqrt{3}}\sum_{\langle\langle i,j\rangle\rangle\alpha\beta} \nu_{ij}c^{\dagger}_{i\alpha}\sigma^{z}c_{j\beta} + U\sum_{i\in C,\alpha} c^{\dagger}_{i\alpha}c_{i\alpha}, \quad (1)$$

where $c^{\dagger}_{i\alpha(\beta)}/c_{i\alpha(\beta)}$ creates/annihilates an electron with spin polarization $\alpha(\beta)$ at site $i$. The indices $\langle i,j\rangle/\langle\langle i,j\rangle\rangle$ run over all the nearest/next-nearest neighbor hopping sites and $i \in C$ represents the sites at the central device. The first term describes the nearest-neighbor hopping of the electrons with $t = 1.6$ eV. The second term represents the effective SOC with strength $\lambda_{SO}$, where $\nu_{ij} = \pm 1$ for the next-nearest-neighbor hopping counterclockwise/clockwise around a hexagon with respect to the positive $z$ axis, and $\sigma^z$ is the Pauli matrix in the $z$ axis. The third term is homogeneous electric field acting as a rectangle electrostatic potential barrier, which is only applied at the central device region to adjust the propagating channel numbers as shown by the yellow block in Fig. 1. Consequently, the electrostatic potential is $U$ at the central device and zero at leads and interfaces. Staggered electric field and exchange field which break the inversion symmetry of system are not considered in the system, so that the bandstructures are in QSH phase and spin-degenerated for both the lead and central device region. As a result, the conductance and valley polarization for spin-up and spin-down electrons are also degenerated. The vanishingly small Rashba SOC at the $K$ and $K'$ point of the bandstructure is excluded in this system.[34]

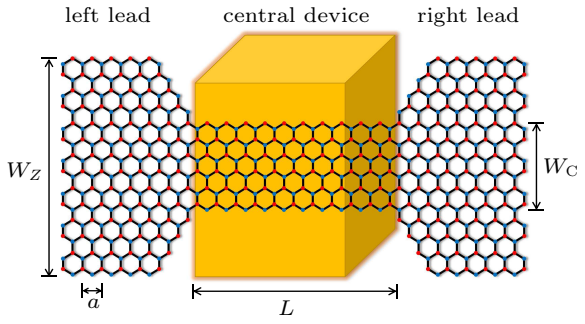



**Fig. 1.** Geometry of silicene nanoconstriction acting as a valley filter consists of quantum point contact with zigzag edges. It is decomposed into three parts: left lead, central device, and right lead. The widths of the lead $W_Z$ tapers down gradually to that of central device $W_C$. The length of the constriction is $L$ and lattice spacing of silicene is $a$. Homogeneous electric field is applied at the central device region (yellow block) to switch polarity of the valley filter.

At low temperature limit, the valley-resolved conductance $G_{K/K'}$ of the silicene nanoconstriction for $K/K'$ valley is given by the Landauer formula,

$$G_{K/K'} = \frac{e^2}{\hbar}\sum_{mn,\alpha}|t_{mn,\alpha}|^2, \quad m,n \in K/K', \quad (2)$$

where $t_{mn,\alpha}$ is the transmission amplitude from the incident channel $n$ to the outgoing channel $m$ for electrons with spin $\alpha$. The channel index $n$ goes through all the modes in two valleys and $m$ is only counted for the modes in a single $K/K'$ valley. The total conductance $G = G_K + G_{K'}$ is the sum of the two valley-resolved conductance. With the Hamiltonian of the system obtained from Eq. (1), the retarded Green function for central device together with two interface parts can be defined by $\mathcal{G}^r_D = (EI - \mathcal{H}_D - \Sigma_L - \Sigma_R)^{-1}$, where $\mathcal{H}_D$ is the Hamiltonian matrix with its dimension equal to the number of atoms inside the corresponding area, $E$ is Fermi energy and $I$ is the identity matrix. The self-energy $\Sigma_L/\Sigma_R$ of the left/right infinite lead can be calculated by the recursive Green function method.[7,41,42] The detailed transmission amplitude $t_{mn,\alpha}$ in terms of Fermi energy $E$ and electrostatic potential $U$ is then accessible by employing Green's function into the mode-matching method.[30,43–45] The procedure starts from solving a quadratic eigenvalue equation derived from the Schrödinger equation to get real (complex) values of wave number for propagating (evanescent) modes, as well as the corresponding wavefunction. For propagating modes, the group velocities of Bloch waves are also calculated to distinguish the directions of propagation (left-going and right-going). Then the propagating modes are sorted into two groups ($K$ and $K'$ valleys), according to their wave number belonging to $(0, \pi/a)$ or $(\pi/a, 2\pi/a)$. Finally, the detailed transmission amplitudes of different valleys are calculated with the wavefunction and Green's function.

With valley-resolved conductance calculated, the valley polarization of transmitted current can be written as

$$P = \frac{G_K - G_{K'}}{G_K + G_{K'}}, \quad (3)$$

where perfect valley filter efficiency $P = \pm 1$ indicates that the propagating modes allowed in the system are fully at the $K/K'$ valley.

## 3. Results and discussion

The size of the silicene nanoconstriction as shown in Fig. 1 is given by $W_Z = 40\sqrt{3}a$, $L = 34a$, $W_C = 20\sqrt{3}a$ in the calculations below. The SOC strength $\lambda_{SO}$ in low-buckled silicene is expected to be 3.9 meV, which becomes larger with the increase of buckled angle.[29] In the case of other group IVA elements such as germanium and tin, the SOC strength is about tens times greater than that of silicene. Specifically, it is $\lambda_{SO} = 0.3$ eV$= 0.15t$ with hopping energy $t = 2$ eV in fluorinated stanene (monolayer of tin).[46,47] The stronger SOC

leads to a larger energy gap at Dirac point, which can better reveal how SOC affects the valley filter efficiency. Therefore, we take $\lambda_{SO} = 0.06t$ and $\lambda_{SO} = 0.12t$ in the silicene system for illustrations of the results. The electrochemical potential over the central device is set as $\mu_0 = E_F - U$, where $E_F$ is Fermi energy of electron and $U$ is the electrostatic potential energy.

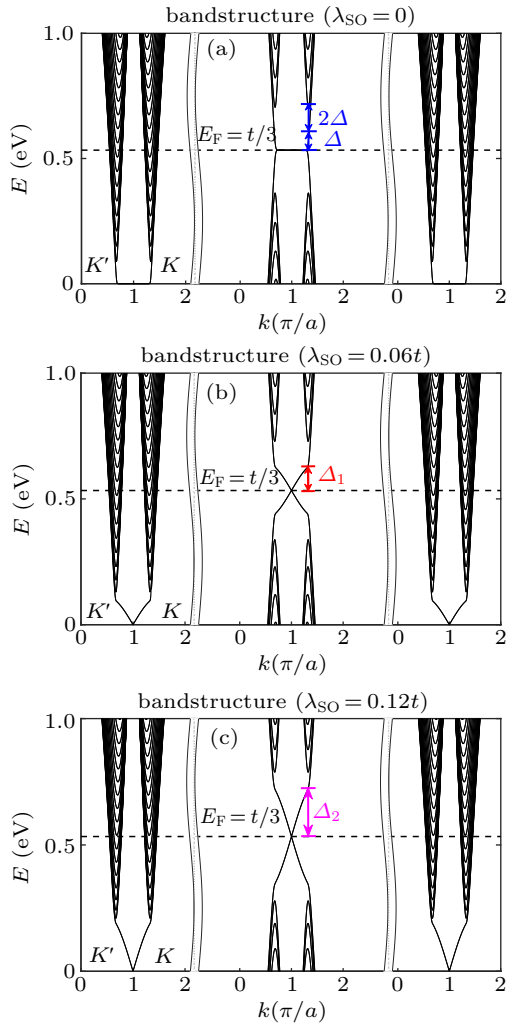



**Fig. 2.** The bandstructure in the left lead, central device and right lead of the silicene nanoconstriction at $\mu_0 = 0$ with spin–orbit coupling strength (a) $\lambda_{SO} = 0$, (b) $\lambda_{SO} = 0.06t$, (c) $\lambda_{SO} = 0.12t$. The Fermi energy is $E_F = t/3$ and homogenous electrostatic potential is $U = t/3$ at the central device region. The energy spacings between the lowest modes and Fermi energy at the two valleys in the central device (half the energy gap between conductance band and valence band at $K/K'$ point) are denoted by $\Delta$, $\Delta_1$ and $\Delta_2$, respectively.

The bandstructure for the three parts of the valley filter device is plotted in Fig. 2. The left and right valleys with central point at wavenumber $k = 2\pi/3a$ and $k = 4\pi/3a$ are denoted by $K'$ and $K$, respectively. The Fermi energy goes exactly through the $\Gamma$ point ($k = \pi/a$) of the bandstructure in the central device region at $\mu_0 = 0$. The lead region supports 17 propagating channels at Fermi energy $E_F = t/3$ without SOC (graphene-like case) as shown in Fig. 2(a). With SOC considered, the number of propagating channels in the lead region remains 17 with SOC strength $\lambda_{SO} = 0.06t$, while decreases to 15 under the condition of SOC strength $\lambda_{SO} = 0.12t$, as shown in Figs. 2(b) and 2(c), respectively. The main reason is that the subband energies in the conduction band are lifted by SOC as the system turns into QSH phase. As shown in Fig. 3, the lowest eigenvalue at $K$ or $K'$ point in the central device increases as SOC is strengthened, and the energy spacing between every two nearest eigenvalues is suppressed. Three typical lowest eigenvalues at $\lambda_{SO} = 0$, $0.06t$ and $0.12t$ are denoted by $\Delta$, $\Delta_1$ and $\Delta_2$, respectively. The energy spacing for the low-lying modes without considering SOC is $2\Delta$, which equals $\sqrt{3}\pi ta/2W_c$ for $W_c/a \gg 1$. As the SOC increases, the subbands becomes denser and energy spacing between the low-lying modes diminishes.

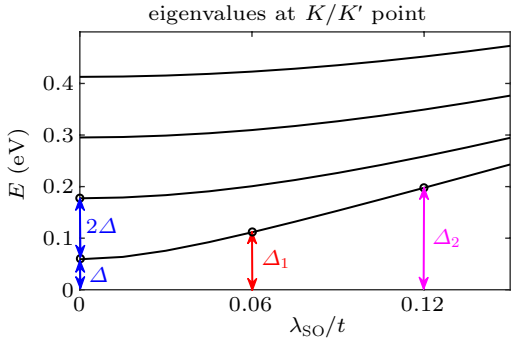



**Fig. 3.** The four lowest eigenvalues at $K/K'$ point in the bandstructure of the central device as a function of spin–orbit coupling strength $\lambda_{SO}$. The magnitude of $\lambda_{SO}$ is in units of the nearest neighbour hopping energy $t$. The energy spacings $\Delta$, $\Delta_1$, $\Delta_2$ are also found in the bandstructure of the central device.

The total conductance $G$ and valley-resolved conductance $G_K$, $G_{K'}$ as a function of the electrochemical potential $\mu_0$ are depicted in Figs. 4 and 5, respectively. As shown in Fig. 4, the plateaus of quantized conductance $G = (2N+1) \times 2e^2/h$ at positive $\mu_0$ holds on, even as SOC is considered. Here $N$ is a non-negative integer and $2N+1$ represents the total number of propagating modes in the central device. The widths of conductance plateaus are determined by the energy spacing of the subbands at $K$ or $K'$ point in the central device. Especially, the first conductance plateau of the graphene-like case in the positive region ($3\Delta$) is broadened due to SOC, which is related to the second lowest subband energy in Fig. 3. In addition, the resonance dip of the total conductance in the negative $\mu_0$ region in the graphene-like case is flattened by SOC because quasi-bound state in the valence band[2] turns into robust QSH edge state. In Fig. 5(a), $G_K$ and $G_{K'}$ in the graphene-like case show good valley selectivity at small $\mu_0$. The first conductance step appears at $\mu_0 = 3\Delta$ for both $G_K$ and $G_{K'}$, where the channel of the second subband in the central device opens. In Figs. 5(b) and 5(c), instead of step-like plateaus, both $G_K$ and $G_{K'}$ show smooth variation at small $\mu_0$ due to the existence of SOC. This means that the propagating modes in both valleys participate in the electronic transport. The turning points for $G_K$ and $G_{K'}$ to quantized conductance plateaus are at $\mu = \Delta_1$

and $\Delta_2$ for $\lambda_{SO} = 0.06t$ and $0.12t$, respectively, which are related to the sudden change of group velocity at $K$ or $K'$ point for the QSH edge state in the bandstructure of central device as shown in Fig. 2.

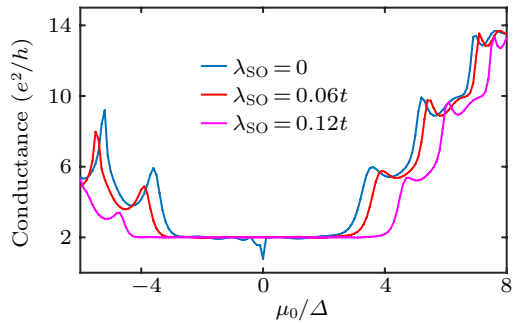



**Fig. 4.** Total conductance $G$ as a function of the electrochemical potential $\mu_0$ for the silicene nanoconstriction. The modes are spin degenerated and the unit of conductance is $e^2/h$. The magnitude of $\mu_0$ is scaled by $\Delta$. The blue, red and magenta lines denote the case of spin–orbit coupling strengths $\lambda_{SO} = 0$, $\lambda_{SO} = 0.06t$, and $\lambda_{SO} = 0.12t$, respectively.

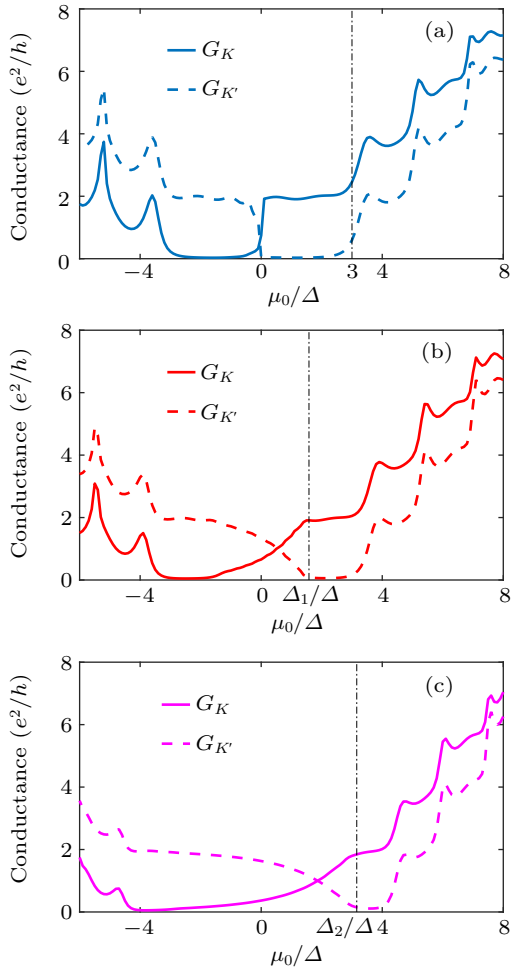



**Fig. 5.** Valley-resolved conductance $G_K$ (full line) and $G_{K'}$ (dashed line) as a function of the electrochemical potential $\mu_0$ for the silicene nanoconstrictions. The blue, red and magenta lines denote the case of spin–orbit coupling strengths (a) $\lambda_{SO} = 0$, (b) $\lambda_{SO} = 0.06t$, (c) $\lambda_{SO} = 0.12t$, respectively.

The valley polarization as a function of the electrochemical potential $\mu_0$ is depicted in Fig. 6. As a positive $\mu_0$ is tuned larger than the eigenvalue of lowest subband at $K$ or $K'$ point in the central device, the polarization shows fractional plateaus $P = 1/(2N+1)$. The ratio of two valley-resolved conductances is $G_{K'}/G_K = N/(N+1)$, where $N$ and $N+1$ are the number of propagating modes for $K'$ and $K$ valley in the central device, respectively. The perfect valley filter efficiency $P = 1$ is achieved as only one right-going propagating channel in the $K$ valley is allowed in the central device, which is the case of $N = 0$. Compared with the graphene-like case, the polarization plateaus is shifted as SOC is strengthened, which corresponds to the conductance step shown in Fig. 4. At small $\mu_0$ with only the QSH edge state allowed as the channel in the central device, the polarization changes smoothly for $\lambda_{SO} = 0.06t$ and $\lambda_{SO} = 0.12t$, instead of a abrupt transition of polarization reversal for $\lambda_{SO} = 0$. Therefore, in the presence of SOC, consecutively tunable valley filter efficiency from negative to positive values can be achieved by aligning the homogenous electric field in the central device. Larger SOC improves the resolution of valley polarization under the same increment of electrochemical potential.

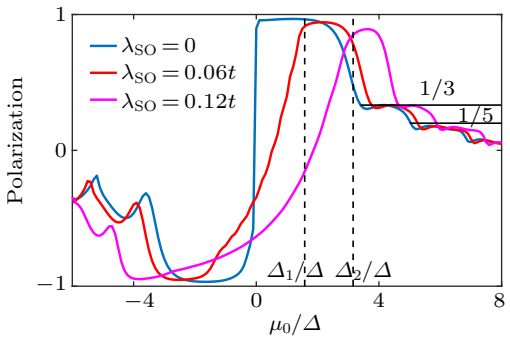



**Fig. 6.** Valley polarization as a function of the electrochemical potential $\mu_0$ for the silicene nanoconstriction. The blue, red and magenta lines denote the case of spin–orbit coupling strengths $\lambda_{SO} = 0$, $\lambda_{SO} = 0.06t$, and $\lambda_{SO} = 0.12t$, respectively.

The valley polarization at $\mu_0 = 0$ becomes smaller than zero for $\lambda_{SO} = 0.06t$, and even smaller for $\lambda_{SO} = 0.12t$, which means $G_{K'}$ dominates the valley filter efficiency with SOC considered. This phenomenon can be intuitively explained by matching the propagating modes at two separate valleys in the leads and the QSH edge state channel in the central device. Take the case of $\lambda_{SO} = 0.12t$ as an example. The zoomed-in bandstructure of the leads is shown in Fig. 7(a), where the right-going propagating modes are labeled in two magenta boxes. The modes lying in the region of $(4\pi/3a, 2\pi/a)$ for the $K$ valley are labeled by $n = 0, 1, \ldots, 7$ from the right-most to the left-most, and the modes lying in the region of $(2\pi/3a, \pi/a)$ for the $K'$ valley are labeled by $n = -1, -2, \ldots, -7$ from the right-most to the left-most. Among all the propagating modes, those in the $K'$ valley are closer to $\Gamma$ point than in the $K$ valley, which have greater possibilities to transmit through the central device. To be specific, the mode-detailed spin-degenerate conductances for each propagating mode are shown in Fig. 7(b). The modes in

the $K$ valley ($G_0, G_1, \ldots, G_7$ in top two rows) have little contribution to conductance at $\mu_0 = 0$. In contrast, the modes in the $K'$ valley (in bottom two rows, especially $G_{-1}$, $G_{-2}$, $G_{-3}$) show greater conductances at $\mu_0 = 0$. Consequently, the sum of conductances for the modes in the $K'$ valley ($G_{K'}$) is greater than that of the $K$ valley ($G_K$) as shown in Fig. 5, leading to negative polarization.

This behavior demonstrates that valley-mixed scattering exists in the valley filter with SOC taked into accounted. In addition, larger SOC in the system makes the group velocity of QSH edge state channel faster at the central device. Therefore, the modes at $K'$ valley are more and more conductive at $\mu_0 = 0$ with the increase of SOC, resulting in smaller negative polarization. Moreover, nearly full valley filter efficiency is also reached at the first plateau as nonzero SOC exists. The critical values of $\mu_0$ for the valley polarization growing to the first plateaus are $\Delta_1$ and $\Delta_2$ for $\lambda_{SO} = 0.06t$ and $0.12t$ respectively, where the Fermi energy goes through the Dirac point of the QSH edge state in the central device. At larger $\mu_0$, the silicene nanoconstrictions have almost the same valley filter effect as the graphene-like case, except the plateaus shift depending on the strength of SOC.

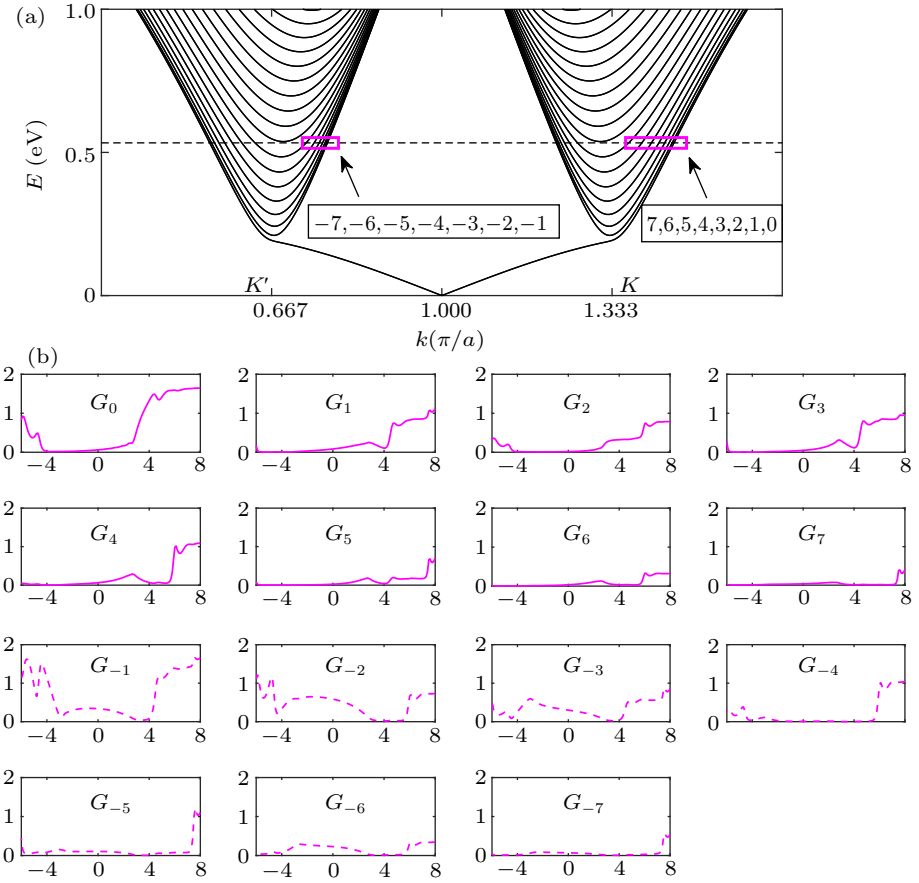



**Fig. 7.** (a) The zoomed-in bandstructure for the leads at Fermi energy $E_F = t/3$ (dashed line) with spin–orbit coupling strength $\lambda_{SO} = 0.12t$. Two magenta boxes are depicted to separate the right-going propagating modes in the $K$ and $K'$ valleys. The modes in the $K$ valley are labeled by $n = 0, 1, \ldots, 7$ from the right-most to the left-most, and the modes in the $K'$ valley are labeled by $n = -1, -2, \ldots, -7$ from the right-most to the left-most. (b) Mode-detailed spin-degenerate conductances (in units of $e^2/h$) for the right-going propagating modes in the leads as a function of the electrochemical potential $\mu_0$ (in units of $\Delta$). The conductances (full line) in top two rows are for the $K$ valley and the conductances (dashed line) in bottom two rows are for the $K'$ valley.

## 4. Conclusion

In summary, we have studied valley-dependent transport properties controlled by SOC in silicene nanoconstrictions. The valley polarization calculated by numerical method shows remarkable valley filter effects as the graphene-like case. However, SOC leads to valley-mixed scattering in silicene nanoconstrictions, which provides consecutively tunable and wide-range valley filter efficiency around Dirac point with only QSH edge state mode allowed in the channel. The lowest conductance step is both flattened and broadened due to SOC, implying robust charge transport in zigzag-edge silicene nanoconstrictions. As the homogeneous gate potential is gradually tuned, quantized conductance steps and valley polarization plateaus are obtained. The position and length of the plateaus are determined by the strength of SOC. Generally, similar valley filter behavior should also be found in devices constructed by other group IVA elements such as germanium and tin. The models proposed here are versatile for different elements with different bond parameters and geometries. Our work may provide insights for designing valleytronic devices

with tunable valley filter efficiency by SOC.

## References


[1] Schaibley J R, Yu H, Clark G, Rivera P, Ross J S, Seyler K L, Yao W and Xu X 2016 *Nat. Rev. Mater.* **1** 16055
[2] Rycerz A, Tworzydło J and Beenakker C W J 2007 *Nat. Phys.* **3** 172
[3] Di X, Yao W and Niu Q 2007 *Phys. Rev. Lett.* **99** 236809
[4] Ang Y S, Yang S, Zhang C, Ma Z and Ang L K 2018 *Phys. Rev. B* **96** 245410
[5] Li J, Zhang R X, Yin Z, Zhang J, Watanabe K, Taniguchi T, Liu C and Zhu J 2018 *Science* **362** 1149
[6] Rycerz A 2008 *Phys. Status Solidi A* **205** 1281
[7] Tsai W F, Huang C Y, Chang T R, Lin H, Jeng H T and Bansil A 2013 *Nat. Commun.* **4** 1500
[8] Settnes M, Power S R, Brandbyge M and Jauho A P 2016 *Phys. Rev. Lett.* **117** 276801
[9] Jia P, Chen W, Qiao J, Zhang M, Zheng X, Xue Z, Liang R, Tian C, He L, Di Z and Wang W 2019 *Nat. Commun.* **10** 3127
[10] Pan H, Li X, Zhang F and Yang S A 2015 *Phys. Rev. B* **92** 041404
[11] Cheng S G, Zhou J, Jiang H and Sun Q F 2016 *New J. Phys.* **18** 103024
[12] Jones G W, Bahamon D A, Neto A H C and Pereira V M 2017 *Nano Lett.* **17** 5304
[13] Suszalski D, Rut G and Rycerz A 2020 *J. Phys. Mater.* **3** 015006
[14] Wang H and Wang J 2018 *Chin. Phys. B* **27** 107402
[15] Yesilyurt C, Siu Z B, Tan S G, Liang G, Yang S A and Jalil M B A 2019 *Sci. Rep.* **9** 4480
[16] Milovanović S P and Peeters F M 2016 *Appl. Phys. Lett.* **109** 203108
[17] Torres V, Silva P, de Souza E A T, Silva L A and Bahamon D A 2019 *Phys. Rev. B* **100** 205411
[18] Faria D, León C, Lima L R F, Latgé A and Sandler N 2020 *Phys. Rev. B* **101** 081410
[19] Mak K F, McGill K L, Park J and McEuen P L 2014 *Science* **344** 1489
[20] Ye Z, Sun D and Heinz T F 2017 *Nat. Phys.* **13** 26
[21] Li H K, Fong K Y, Zhu H, Li Q, Wang S, Yang S, Wang Y and Zhang X 2019 *Nat. Photon.* **13** 397
[22] Aivazian G, Gong Z, Jones A M, Chu R L, Yan J, Mandrus D G, Zhang C, Cobden D, Yao W and Xu X 2015 *Nat. Phys.* **11** 148
[23] Wang J J, Liu S, Wang J and Liu J F 2018 *Phys. Rev. B* **98** 195436
[24] Kim Y and Lee J D 2019 *Nano Lett.* **19** 4166
[25] Ye Y, Xiao J, Wang H, Ye Z, Zhu H, Zhao M, Wang Y, Zhao J, Yin X and Zhang X 2016 *Nat. Nanotechnol.* **11** 598
[26] Hsieh T C, Chou M Y and Wu Y S 2018 *Phy. Rev. Mater.* **2** 034003
[27] Qi P and Mi W 2019 *Phys. Rev. Appl.* **11** 14011
[28] Grujić M M, Tadić M Ž and Peeters F M 2014 *Phys. Rev. Lett.* **113** 46601
[29] Liu C C, Jiang H and Yao Y 2011 *Phys. Rev. B* **84** 195430
[30] Li Y, Zhu H B, Wang G Q, Peng Y Z, Xu J R, Qian Z H, Bai R, Zhou G H, Yesilyurt C, Siu Z B and Jalil M B A 2018 *Phys. Rev. B* **97** 085427
[31] Premasiri K and Gao X P A 2019 *J. Phys.: Condens. Matter* **31** 193001
[32] Kane C L and Mele E J 2005 *Phys. Rev. Lett.* **95** 226801
[33] Liu C C, Feng W and Yao Y 2011 *Phys. Rev. Lett.* **107** 76802
[34] Ezawa M 2013 *Appl. Phys. Lett.* **102** 172103
[35] Bernevig B A, Hughes T L and Zhang S C 2006 *Science* **314** 1757
[36] An X T, Zhang Y Y, Liu J J and Li S S 2013 *Appl. Phys. Lett.* **102** 43113
[37] Wu S, Fatemi V, Gibson Q D, Watanabe K, Taniguchi T, Cava R J and Jarillo-Herrero P 2018 *Science* **359** 76
[38] Qian X, Liu J, Fu L and Li J 2013 *Science* **346** 1344
[39] Yesilyurt C, Tan S G, Liang G, and Jalil M B A 2015 *Appl. Phys. Express* **8** 105201
[40] Wang S K and Wang J 2015 *Chin. Phys. B* **24** 037202
[41] Khomyakov P A, Brocks G, Karpan V, Zwierzycki M and Kelly P J 2005 *Phys. Rev. B* **72** 35450
[42] Lan J, Ye E J, Sui W Q and Zhao X A 2013 *Phys. Chem. Chem. Phys.* **15** 671
[43] Li Y, Jiang W Q, Ding G Y, Peng Y Z, Wen Z C, Wang G Q, Bai R, Qian Z H, Xiao X B and Zhou G H 2019 *J. Appl. Phys.* **125** 244304
[44] Jin C L, Lan J, Zhao X A and Sui W Q 2016 *Eur. Phys. J. B* **89** 187
[45] Ando T 1991 *Phys. Rev. B* **44** 8017
[46] Rachel S and Ezawa M 2014 *Phys. Rev. B* **89** 195303
[47] Lü X L, Xie Y and Xie H 2018 *New J. Phys.* **20** 43054